◆ Human Brain Mapping 22:145–154(2004) ◆

Protocol for Volumetric Segmentation of Medial Temporal Structures Using High-Resolution 3-D Magnetic Resonance Imaging

Leonardo Bonilha, Eliane Kobayashi, Fernando Cendes, and Li Min Li*

Neuroimage Laboratory, Department of Neurology, State University of Campinas, Campinas, Brazil

Abstract: Quantitative analysis of brain structures in normal subjects and in different neurological conditions can be carried out in vivo through magnetic resonance imaging (MRI) volumetric studies. The use of high-resolution MRI combined with image post-processing that allows simultaneous multiplanar view may facilitate volumetric segmentation of temporal lobe structures. We define a protocol for volumetric studies of medial temporal lobe structures using high-resolution MR images and we studied 30 healthy subjects (19 women; mean age, 33 years; age range, 21–55 years). Images underwent field non-homogeneity correction and linear stereotaxic transformation into a standard space. Structures of interest comprised temporopolar, entorhinal, perirhinal, parahippocampal cortices, hippocampus, and the amygdala. Segmentation was carried out with multiplanar assessment. There was no statistically significant left/right-sided asymmetry concerning any structure analyzed. Neither gender nor age influenced the volumes obtained. The coefficient of repeatability showed no significant difference of intra- and interobserver measurements. Imaging post-processing and simultaneous multiplanar view of high-resolution MRI facilitates volumetric assessment of the medial portion of the temporal lobe with strict adherence to anatomic landmarks. This protocol shows no significant inter- and intraobserver variations and thus is reliable for longitudinal studies. *Hum. Brain Mapp. 22:145–154, 2004.* © 2004 Wiley-Liss, Inc.

Key words: magnetic resonance image; temporal lobe; parahippocampal gyrus; volumetric analysis

INTRODUCTION

The amygdala and the hippocampus, together with surrounding cortical areas such as the entorhinal, perirhinal, parahippocampal, and temporopolar cortices, constitute the medial portion of the temporal lobe. These structures function in concert through a large and intricate number of interconnections [Insausti et al., 1987; Watson et al., 1997] and play an important role in carrying out complex behavioral tasks including declarative and representative memory processing [Berkovic et al., 1991; Margerison and Corsellis, 1966; Squire and Zola-Morgan, 1991; Suzuki and Amaral, 1994].

The hippocampus and the amygdala constitute the core of the limbic system. Due to its extensive connections, the hippocampus is thought to be the center for memory and learning functions [Gloor, 1997; Milner, 1972, 1970; Scoville and Milner, 1957]. In primates, hippocampal cortical connections involve mainly the isocortical association cortex located in frontal, parietal, and temporal lobes. These connections are mediated in both directions by the entorhinal cortex and in the efferent portion by the subicular complex. Afferent cortical projections to the entorhinal cortex come from multimodal cortical association areas, particularly from the perirhinal and parahippocampal cortices, which are associated closely with the entorhinal cortex both functionally and anatomically [Squire and Zola-Morgan, 1991].

Contract grant sponsor: FAPESP; Contract grant number: 00/04710-2.

*Correspondence to: Li Li Min, Department of Neurology, Faculty of Medicine, UNICAMP, 13083-970, Campinas, SP, Brazil.
E-mail: limin@fcm.unicamp.br

Received for publication 1 November 2002; Accepted 17 December 2003

DOI 10.1002/hbm.20023

Lesions carried out stereotactically to amygdala, hippocampus, and to adjacent and anatomically related cortices, have demonstrated that the temporal lobe memory system is established over an intricate network connecting the hippocampus, the perirhinal, the entorhinal, and the parahippocampal cortex [Mishkin, 1978; Squire et al., 1980; Zola-Morgan and Squire, 1985]. These findings have confirmed previous clinical observations of memory impairment in those patients with lesions of the medial portion of the temporal lobe [Milner, 1972], and have refined the definition of anatomical components and connections of the primate temporal lobe [Jack, 1994; Zola-Morgan et al., 1986]. The precise function, however, of each temporal lobe structure in normal cognitive function or their relevance in pathological conditions has yet to be determined fully [Gloor, 1997].

The possibility of volumetric studies through magnetic resonance imaging (MRI) allows noninvasive studies of brain anatomy in vivo. Analysis of brain structures in normal subjects and patients with different neurological conditions therefore can shed light on the physiopathology of diseases [Jackson et al., 1990; Pruessner et al., 2000; Seidman et al., 1999; Xu et al., 2000]. For example, amygdala or hippocampal MR-based volumetric analysis has been used successfully to determine tissue damage, particularly in temporal lobe epilepsy [Cendes et al., 1993]. There are currently a limited number of protocols available for studying other temporal lobe structures such as parahippocampal gyrus [Bronen et al., 1991] or the entorhinal cortex [Bernasconi et al., 1999]. Segmentation of medial temporal structures, particularly cortical components, poses some difficulties in regard to definition of their anatomical boundaries. This issue can be overcome in part with the use of high-resolution MRI combined with image post-processing analysis that allows simultaneous multiplanar view [Pruessner et al., 2000].

We present a segmentation protocol for medial temporal cortices based on anatomic guidelines developed through histological assessment [Gloor, 1997; Insausti et al., 1998; Watson et al., 1992] and a previous high-resolution MRI protocol of amygdalae and hippocampi segmentation [Pruessner et al., 2000]. This protocol was developed for high-resolution image acquisition and segmentation software with multiplanar view.

SUBJECTS AND METHODS

Subjects

We studied 30 healthy subjects (19 women; mean age, 33 years; age range, 22–55 years). All were in good health and did not have any previous medical history of neurological or psychiatric disorders. This study and procedures was approved by the ethics committee of our Institution.

MRI Acquisition

We used T1-weighted images with 1-mm isotropic voxel obtained using a 3D spoiled gradient-echo acquisition with sagittal volume excitation (TR = 22 msec, TE = 9 msec, matrix = 256 × 220, field of view [FOV] = 25 × 25 cm, 1-mm sagittal slices). All images were obtained in a 2T scanner (Elscint Prestige, Haifa, Israel).

Image Post-Processing

All scans were transferred to a O_2 workstation (Silicon Graphics, Mountain View, CA). Different algorithms from the McConnell Brain Imaging Centre (Montreal, Canada) were used to prepare raw MRI volume for quantitative and qualitative analysis. First, raw images were converted into the "minc" electronic file format (see http://www.bic.mni.mcgill.ca/software/minc/minc.html). Second, images were automatically registered into stereotaxic space [Talairach and Tornoux, 1988] to adjust for differences in brain volume and orientation and to minimize variability in slice orientation [Collins et al., 1994; Lancaster et al., 1995; Paus et al., 1996; Penhune et al., 1996]. Third, images were corrected for field nonuniformity using the N3 software program (online at http://www.bic.mni.mcgill.ca/software/N3/) [Sled et al., 1998].

Volumetric Analysis

Segmentation was carried out with the interactive software package DISPLAY (developed by David McDonald) developed at the Brain Imaging Centre of the Montreal Neurological Institute. Delineating anatomical boundaries is facilitated by contrast adjustment and the possibility for navigation through isotropic voxels of 1 mm in different orientations with the same resolution. The software automatically calculates volumes of labeled structures. Despite the possibility of semiautomatic quantification of anatomical regions of interest, we decided to carry out manual delineation of each structure, to enhance the accuracy of the measurement.

The volumes were determined by two observers (L.B. and E.K.). All landmarks were based on previously published studies that addressed histological or anatomical features of the medial and anterior portion of the temporal lobe [Gloor, 1997; Insausti et al., 1998; Pruessner et al., 2000; Watson et al., 1992]. We defined a protocol that could be carried out easily with a quick reference to the axial, sagittal, and coronal planes to accurately define and insure the location of the anatomical landmarks, which otherwise would be delineated with difficulties on a single-plane based morphometric study [Gloor, 1997; Insausti et al., 1998; Pruessner et al., 2000; Watson et al., 1992].

Reliability Assessment

Intraobserver reliability was evaluated by random selection of five subjects and segmentation of all structures twice within a 30-day interval. Inter-rater reliability was assessed by comparison of volumes of all structures from five randomly chosen subjects carried out by the two observers (L.B. and E.K.) who were each blind to results obtained by the other.

The use of a correlation coefficient can be misleading by showing how measurements are correlated rather than

showing if they are similar [Bland and Altman, 1986]. If one form of measurement is the same as another form of measurement multiplied by a constant, these two forms of measurement are perfectly correlated although they are not similar. We therefore used the repeatability coefficient adopted by The British Standards Institution [Bland and Altman, 1986] calculated by the standard deviation of the differences to assess intra-rater and inter-rater reliability for these subjects. We assumed the mean difference to be zero, and calculated the coefficient by adding the square of the differences between the two different measurements. The result was the square root of sum of the squares of the differences divided by n. To conclude that there was not significant difference between the measurements, we expected that 95% of the differences were less than two standard deviations [Bland and Altman, 1986].

Statistical Analysis

Data was evaluated using SYSTAT for Windows v. 9.0 (Systat, Point Richmond, CA). We described the minimum, maximum, mean, and standard deviation for volumes of the structures analyzed. We used Student's *t*-test to calculate mean age difference grouped by gender. Multivariate analysis of variance (MANOVA) was used for comparison of volume results grouped by gender. To evaluate the mean side-to-side volume difference of each structure, we also applied MANOVA with two within-subject factors (side: left, right; structures: temporopolar cortex, perirhinal cortex, entorhinal cortex, parahippocampal cortex, hippocampus, and amygdala). We used linear regression for correlation between age and the volume results. The level of statistic significance was set at $P < 0.05$.

Segmentation Protocol

The coronal plane was the starting point, because most landmarks can be defined in this plane. Doubts concerning the authenticity of the structure visualized were resolved by the concomitant visualization in the two other planes. Specific structures posed remarkable difficulty for definition in the coronal plane. For these structures, visualization of sagittal and axial planes were required and used as the starting point.

In the definition of anatomical landmarks below, we have considered that the transverse gyrus of Schwalbe is defined as the gyrus lateral to the temporopolar sulcus, the lateral sulcus closure is defined by the unequivocal junction of frontal and temporal lobes, and the intralimbic gyrus is defined in the sagittal plane by the first section after the posterior end of the limbus of Giacomini. The rhinal sulcus is an anterior and discontinued branch of the collateral sulcus, present at the anterior portion of the parahippocampal gyrus. For segmentation purposes, it is not necessary to discriminate between the rhinal and collateral sulcus. Boundaries of anatomical regions of interest located in the collateral sulcus were also located in precisely the same way in the rhinal sulcus. For that reason, in the segmentation protocol we use the term collateral sulcus to refer to both the collateral sulcus and to its anterior extension, the rhinal sulcus. The structures that were defined a priori in the sagittal plane were the collateral sulcus, the calcarine fissure, and the alveus. The definition of the sulci parts used in the protocol is displayed in Figure 1. The steps followed during the segmentation process are described below.

Temporopolar cortex

The segmentation of the temporopolar cortex follows a rostrocaudal orientation (Fig. 2A–C). In the rostral pole of the temporal lobe, the whole cortex belongs to the temporopolar cortex until the temporopolar sulcus appears defining the transverse gyrus of Schwalbe, which is lateral to the temporopolar sulcus (Fig. 2B). The lateral bank of the transverse gyrus of Schwalbe defines the superior and lateral limit of the temporopolar cortex. Whenever there were two gyri lateral to the temporopolar sulcus, the lateral bank of the most lateral sulcus was defined as the lateral border of the temporopolar cortex. The inferior limit was defined as the medial edge of the occipitotemporal sulcus (Fig. 2B) or the superior temporal sulcus, if the occipitotemporal sulcus was not present. The medial portion of the temporopolar cortex thickens in the caudal direction. A sulcus at this point is usually not seen, but the unequivocal presence of the collateral sulcus is located generally near the lateral sulcus closure. For reasons of consistency, we did not consider this frequent cortical enlargement as the rostral limit of the collateral sulcus, which was observed to appear in most cases 1–2 mm anterior to the lateral sulcus closure. The anterior limit of perirhinal cortex therefore was defined at this point, i.e., the slice 2 mm anterior to the lateral sulcus closure, and the caudal limit of the temporopolar lobe was defined at 3 mm anterior to the lateral sulcus closure.

Entorhinal cortex

The segmentation of the entorhinal cortex follows a rostrocaudal orientation (Fig. 2D–F). The superior limit of the entorhinal cortex is the semiannularis sulcus in the more rostral sections (Fig. 2E). In the caudal sections where the uncal sulcus is visible, the superior limit is defined as the most medial point of the inferior part of the uncal sulcus. The inferior limit is defined as the middle point of the medial bank of the collateral sulcus. The medial limit is the pial surface, whereas the lateral limit is the white matter of the angular bundle. The caudal limit of the entorhinal cortex is the slice 2 mm caudal to the intralimbic gyrus closure.

Perirhinal cortex

The segmentation of the perirhinal cortex follows a rostrocaudal orientation (Fig. 3A–E). The rostral limit of the perirhinal cortex is the slice 2 mm anterior to the lateral sulcus closure. In the two most rostral slices, the perirhinal cortex has the same boundaries as the temporopolar cortex, i.e., the lateral bank of the transverse gyrus of Schwalbe and the medial edge of the occipitotemporal sulcus. In the slice where the lateral sulcus closure is visible and in the slice

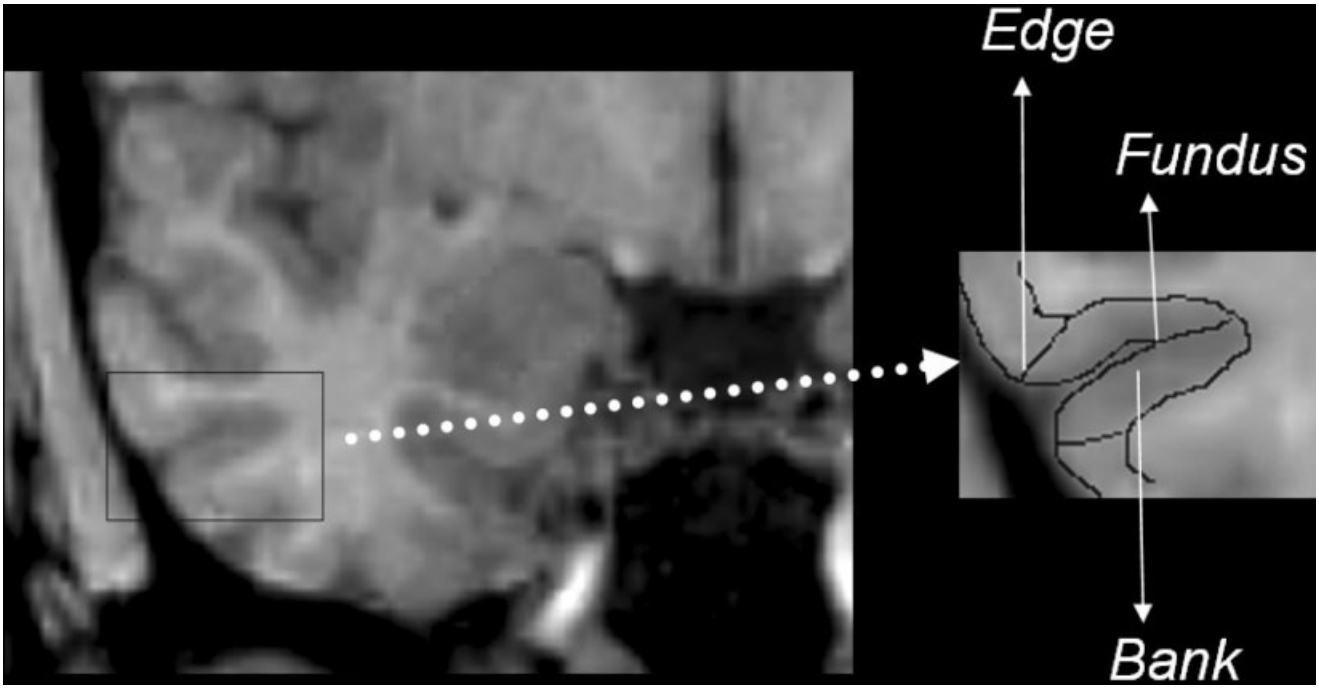

Figure 1.

The figure displays the names of the different parts of the sulci that are used in the segmentation protocol. The right box represents a magnification of the inferior temporal sulcus of the right temporal lobe, and the different parts of the sulcus are labeled. These named parts are equivalent in different sulci.

immediately caudal, the superior limit of the perirhinal cortex is the most medial point of the parahippocampal gyrus, and the inferior limit defined as the lateral edge of the collateral sulcus (Fig. 3A). We decided not to adopt the length of the collateral sulcus as an orientation for altering the perirhinal and entorhinal cortex landmarks because there is great variation in the length of the collateral sulcus in along the temporal lobe. We decided then to carry out all segmentations based on the anatomic landmarks defined for the collateral sulcus with the most frequent pattern [Insausti et al., 1998]. In the slice 2 mm caudal to the closure of lateral sulcus, the superior limit of the perirhinal cortex is a 45-degree oriented line connecting the middle point of the medial aspect of the parahippocampal gyrus, whereas the inferior limit is the lateral edge of the collateral sulcus (Fig. 3B). In the following caudal sections, the inferior limit is defined as the lateral edge of the collateral sulcus until the caudal end, whereas the superior limit is defined as the middle point of the medial bank of the collateral sulcus until the slice 2 mm caudal to intralimbic gyrus closure (Fig. 3C and Fig. 4D). In the section 3 mm and 4 mm caudal to the intralimbic gyrus closure, the superior limit is defined where the gray matter forms a continuum with the underlying angular bundle, i.e., the most medial point of the inferior part of the uncal sulcus. The closure of intralimbic gyrus is defined in the sagittal slices. The caudal limit of the perirhinal cortex is the slice 4 mm posterior to the intralimbic gyrus closure (Fig. 4D).

Parahippocampal cortex

The segmentation of the parahippocampal cortex follows a rostrocaudal orientation (Fig. 4A–C). The lateral limit of the parahippocampal cortex is the edge of the lateral bank of the collateral sulcus, and the medial limit is the most medial point of the inferior part of the uncal sulcus. In more caudal sections, where the calcarine sulcus is present, the medial limit is defined as the most superior point not involving the inferior bank of the calcarine sulcus (Fig. 4B). The calcarine sulcus along with its rostral limit is determined by sagittal sections. The caudal limit of the parahippocampal cortex is the most caudal section containing the hippocampus, i.e., the caudal limit of the hippocampus.

Hippocampus

For the head of the hippocampus, the anterior and superior-lateral borders in the rostral end of hippocampus are difficult to define (Fig. 4D–F). In this region, the gray matter of the hippocampal head merges with the gray matter of the amygdala. The uncal recess of the lateral ventricle, along with the alveus, is used for distinction between the hippocampal head and other structures. A constant reference to all planes is the best approach for delineating the margins. The hippocampal head was defined as continuing one additional row of pixels anterior to the alveus. This was best accomplished with visualization of the sagittal plane and by

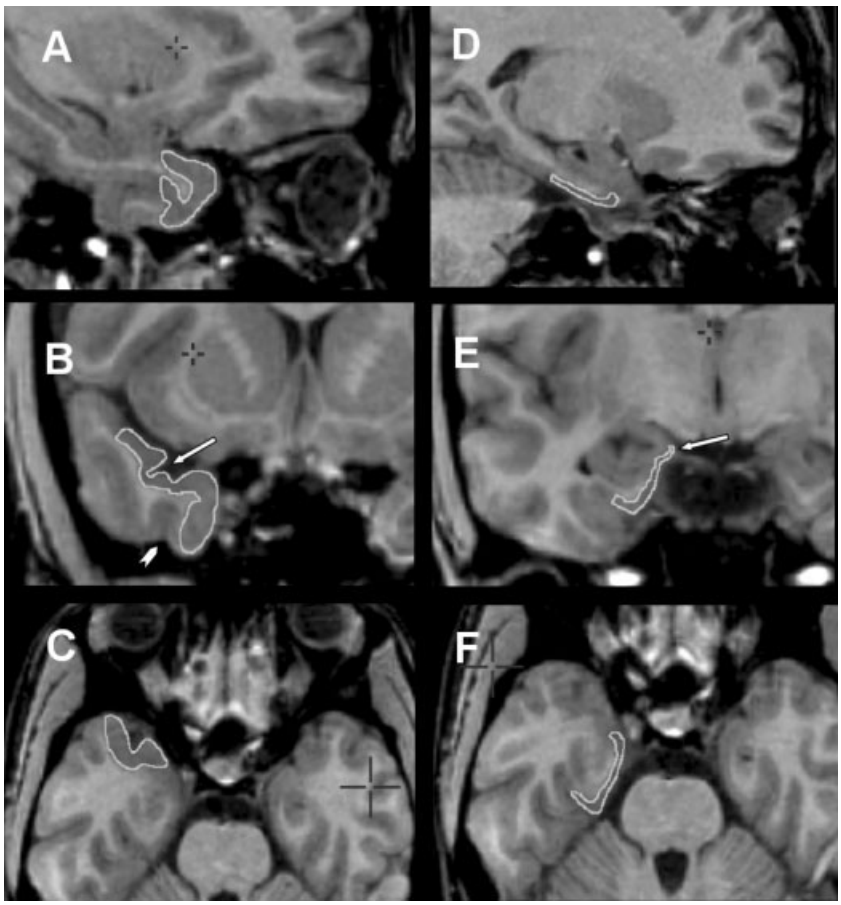

Figure 2.

Composite of MRI showing the temporopolar cortex (**A**, sagittal plane; **B**, coronal plane; **C**, axial plane) and the entorhinal cortex (**D**, sagittal plane; **E**, coronal plane; **F**, axial plane) with anatomic boundaries delineated by edge tracing (see text for description of anatomical landmarks used for segmentation). Both the entorhinal and perirhinal cortices are constant structures, without significant changes in landmarks in the rostrocaudal axis. Arrows indicate key landmarks. B: Arrow indicates temporopolar sulcus and arrowhead indicates occipitotemporal sulcus. E: Arrow indicates the semiannularis sulcus.

definition of the posterior borders of the amygdala in the axial plane (see amygdala segmentation explained below). The inferior border of the hippocampal head was defined as the white and gray matter transition underlying the subiculum or a 45-degree oriented line extending from most inferior part of the hippocampus to the quadrigeminal cistern. A line of white matter separating the subiculum and entorhinal cortex is sometimes visible, and serves as an orienting line. The lateral end of the hippocampal head was the lateral ventricle. For the hippocampal body, the inferior and lateral margins of the hippocampal body were defined as for the hippocampal head. The superior border included the fimbria and the first row of white matter pixels immediately superior to the fimbria. For the hippocampal tail, the hippocampus starts in its caudal end as an oval mass of gray matter inferomedially to the lateral ventricle. Two rows of pixels were excluded laterally because this was considered to be part of the lateral ventricle. To prevent the Andreas-Retzius gyrus from being included in the segmentation, we applied a line connecting the medial point of the lateral ventricle and the parahippocampal gyrus. This line served as a medial border. In addition, to prevent the inclusion of the fasciolar gyrus in the segmentation, we defined the superior margin as a horizontal line connecting the most lateral point of the quadrigeminal cistern to the lateral ventricle. The inferolateral borders of the hippocampal tail were easily defined by the transition to white matter. One row of pixels was excluded from the inferolateral border to exclude the tail of the caudate nucleus and the inferior horn of the lateral ventricle.

Amygdala

For segmentation of the amygdala (Fig. 4G–I), a constant reference of the axial, sagittal, and the coronal planes was used. The best way to define the posteroinferior limits of the amygdala was to visualize the alveus and the lateral ventricle in the axial plane with image magnification (Fig. 4I).

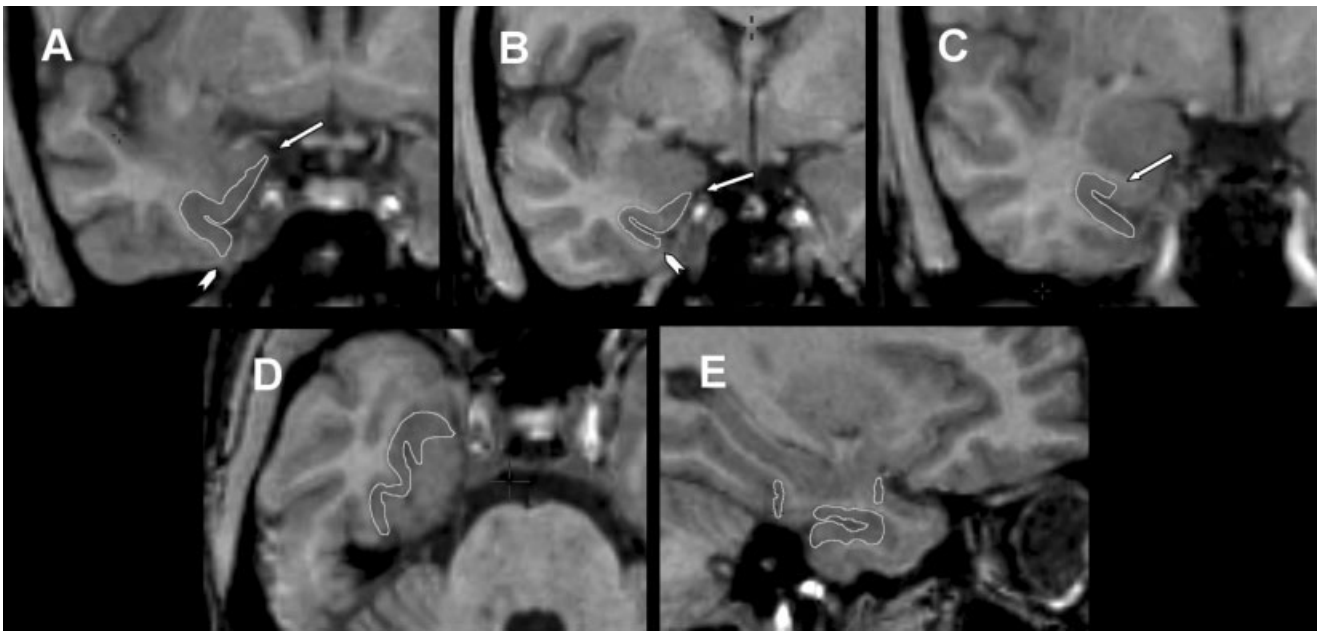

Figure 3.

Composite of MRI showing perirhinal cortex with boundaries delineated by edge tracing (**A– C**, coronal plane; **D**, axial plane; **E**, sagittal plane). The perirhinal cortex has significant changes in boundaries within rostrocaudal axis. A–C: Most constant aspects of the perirhinal cortex in the rostrocaudal sequence; key landmarks are labeled. A: Arrow indicates most medial point of parahippocampal gyrus and arrowhead indicates medial edge of occipitotemporal sulcus. B: Arrow indicates medial point of the medial aspect of parahippocampal gyrus and arrowhead indicates lateral edge of the lateral bank of collateral sulcus. C: Arrow indicates midpoint of the superior bank of collateral sulcus.

After definition of the posteroinferior limits, the anterior limits were defined by a semicircle drawn anteriorly with its radius defined at the middle point of the line drawn over the alveus in the posterior border. There was special care taken to avoid involving the entorhinal cortex. Finally, after definition of boundaries in the axial plane, a thorough rostrocaudal analysis was made in the coronal plane, with particular attention to the superior limit, defined as a horizontal line connecting the most lateral portion of the endorhinal sulcus to the fundus of the circular sulcus of the insulae, and the lateral limit, defined as the white-gray matter transition.

RESULTS

Maximum and minimum volume, mean values, and standard deviation for each structure analyzed are shown in Table I.

Reliability Assessment

The results of the calculations for reliability assessment are shown in Table II. There was no significant difference between the measurements carried out by one or by two raters, because all differences between measurements were less than two standard deviations of differences of the respective structure.

Effects of Gender and Age on Cortical Volumes

There was no difference on age grouped by gender ($t(28) = 0.151$, $P = 0.881$). There was no difference in the volume of structures according to gender (Table III) and we did not observe a significant correlation between the volumes of the structures and age.

Symmetry

There was no significant side-to-side difference in evaluated structures (Table III).

DISCUSSION

We developed a protocol for medial temporal structure segmentation with the use of MR images and multiplanar navigation software. The creation of this new protocol was driven by the necessity of a tool to enhance the accuracy of the volumetric assessment of medial temporal lobe structures. Because many current tools used to analyze the volumes of brain structures rely on a single plane of thick slices of MR images, assessment of the small structures of the temporal lobe can be difficult. In addition, the cortical structures of the temporal lobe have boundaries that do not always rely on surface landmarks, or if so, involve subtle sulci or gyri that are difficult to define in one single plane or in low-resolution images.

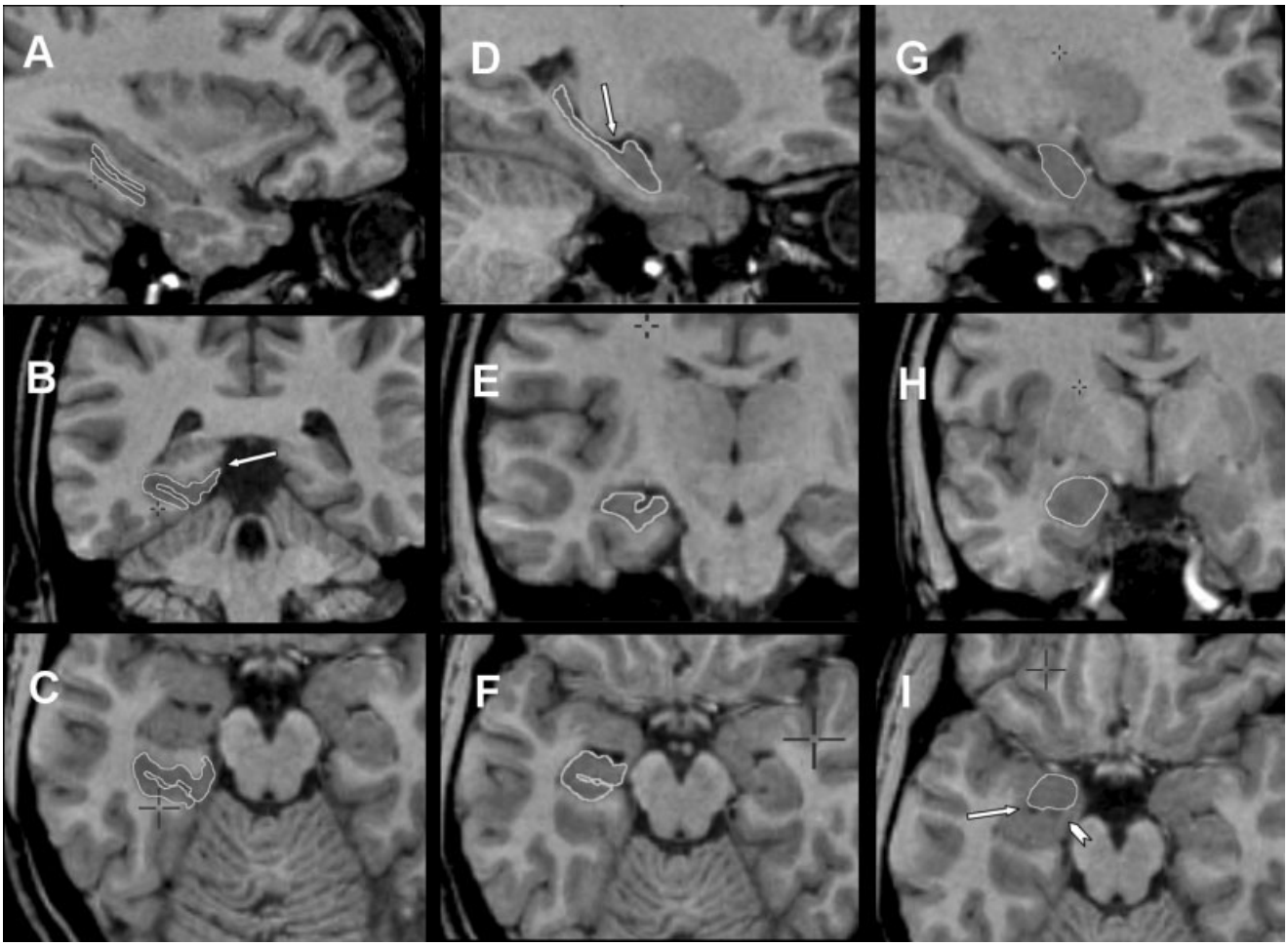

Figure 4.

Composite of MRI showing parahippocampal cortex (**A**, sagittal plane; **B**, coronal plane; **C**, axial plane), hippocampus (**D**, sagittal plane; **E**, coronal plane; **F**, axial plane) and amygdala (**G**, sagittal plane; **H**, coronal plane; **I**, axial plane). Parahippocampal cortex, hippocampus, and amygdala have constant boundaries (refer to text for segmentation steps) and key landmarks are labeled. B: Arrow indicates inferior limit of the inferior bank of calcarine fissure. D: Arrow indicates intralimbic gyrus closure. I: Arrow indicates temporal horn of the lateral ventricle and the arrowhead indicates the alveus.

Some prevalent diseases such as temporal lobe epilepsy, schizophrenia, autism, and Alzheimer's disease involve the temporal lobe in its medial portion. The damage to the hippocampus or amygdala in these conditions is somewhat well established. Nevertheless, the degree of compromise of surrounding cortical structures is not well understood, and the contribution of these areas to physiopathology and symptomatology of these conditions has not yet been determined fully. Hence, the creation of a more powerful tool to assess the volume of this region may be of interest.

The definition of the anatomic landmarks was best accomplished when the structure of interest could be visualized simultaneously in several planes. The landmarks observed in different planes were used conjointly for segmentation and this provided a high level of accuracy and security for the results obtained. A disadvantage of the careful multiplanar analysis was the time devoted to each segmentation. It took on average 4 hr to carry out segmentation of each subject (6 structures for each temporal lobe, 12 structures in total). We believe, however, that continuous training may substantially decrease the time span of the segmentation process.

Another aspect that contributed to enhance the accuracy of image edition was the post-acquisition image processing applied to all images before visual analysis. The images underwent correction for field nonhomogeneity using the program N3, which provided a considerable improvement in the image quality. The N3 software is a nonparametric method for correction of intensity nonuniformity in MRI data and it removes image artifacts [Sled et al., 1998].

The linear stereotaxic transformation was also particularly important because it removes the influence of the whole

TABLE I. Medial temporal lobe structure volumes

	Perirhinal cortex		Temporopolar cortex		Entorhinal cortex		Parahippocampal cortex		Hippocampus		Amygdala	
Subjects	Left	Right	Left	Right	Left	Right	Left	Right	Left	Right	Left	Right
All subjects												
Maximum	3,063	2,860	4,032	4,078	1,660	1,897	2,586	2,273	3,949	3,999	1,946	2,175
Minimum	1,315	1,395	1,987	1,981	703	711	1,227	1,146	2458	2,369	1,108	1,112
Mean	2,256	2,198	3,234	3,133	1,107	1,143	1,620	1,536	3,238	3,222	1,544	1,503
SD	394	438	468	590	266	310	313	303	382	345	247	263
Men												
Maximum	2,881	2,922	4,032	3,962	1,564	1,897	2,250	2,469	1,946	1,846	3,949	3,729
Minimum	2,029	1,953	2,785	2,202	858	819	1,280	1,146	1,046	1,010	2,594	2,710
Mean	2,410	2,333	3,324	3,168	1,165	1,218	1,588	1,505	1,629	1,578	3,089	3,099
SD	337	321	382	562	221	292	316	377	281	272	356	290
Women												
Maximum	3,063	2,860	3,942	4,282	1,660	1,752	2,590	2,572	1,919	2,175	3,901	3,999
Minimum	1,315	1,395	1,987	1,981	703	711	1,227	1,195	1,108	1,112	2,458	2,369
Mean	2,203	2,151	3,196	3,136	1,103	1,132	1,728	1,651	1,509	1,471	3,330	3,315
SD	412	473	513	632	292	324	410	404	225	251	377	386

Maximum and minimum volumes, mean values, and standard deviations (SD) in mm^3.

brain volume over particular structures. The volumes obtained then reflected the size and magnitude of the structure compared to other cerebral regions. The use of a homogeneous group of images may minimize discrepancies between different studies and allow comparison of the effects of certain morbid conditions or normal physiologic process on brain structures, avoiding biases provoked by the corresponding total brain volume and size of particular structures.

Image correction prevented the straight comparison of volumes obtained from this protocol with volumes obtained from previous studies, because some carried out volumetric analysis on raw images or on images submitted to different processes of normalization. In comparison to other studies, the main findings can be grouped as detailed below.

Effects of Gender and Age on Cortical Volumes

We did not observe differences in age when the sample was grouped by gender. There was no difference in volumes obtained when the sample was grouped by gender and there was no linear correlation of volumes with age. Some previ-

TABLE II. Reliability assessment values

	Perirhinal cortex		Entorhinal cortex		Temporopolar cortex		Parahippocampal cortex		Hippocampus		Amygdala	
Measurement (mm^3)	Left	Right	Left	Right	Left	Right	Left	Right	Left	Right	Left	Right
First (n = 5)												
Mean	2,402	2,408	1,181	1,278	3,202	3,194	1,824	1,849	2,981	2,967	1,628	1,708
SD	219	304	163	221	157	411	374	479	289	161	200	306
Reliability assessment												
Intra-observer												
Mean	2,359	2,277	1,113	1,221	3,242	3,203	1,598	1,526	3,061	3,117	1,524	1,545
SD	143	201	159	145	210	305	793	774	279	114	195	286
SD of differences	206	211	117	151	127	205	299	230	179	125	183	269
Repeatability coeff.	412	422	234	302	254	410	598	460	358	250	366	538
Inter-observer												
Mean	2,572	2,511	1,184	1,132	3,157	2,931	1,398	1,582	3,376	3,434	1,485	1,459
SD	238	292	196	185	280	416	247	305	364	362	49	234
SD of differences	186	286	241	135	200	152	227	190	151	199	243	120
Repeatability coeff.	372	572	482	270	400	304	454	380	302	398	486	240

SD, standard deviation; coeff., coefficient.

TABLE III. Evaluation of the volumes of the structures according to gender, age, and symmetry

Structure	Statistical analysis		
	Group differences for gender (MANOVA)	Linear regression with age	Side-to-side difference (MANOVA)
Left perirhinal cortex	$\lambda(58,2) = 1.70$, $P = 0.21$	$r = 0.17$, $P = 0.44$	$\lambda(58,1) = 0.57$, $P = 0.45$
Right perirhinal cortex	$\lambda(58,2) = 2.40$, $P = 0.14$	$r = 0.06$, $P = 0.75$	
Left temporopolar cortex	$\lambda(58,2) = 0.70$, $P = 0.43$	$r = 0.11$, $P = 0.55$	$\lambda(58,1) = 0.29$, $P = 0.59$
Right temporopolar cortex	$\lambda(58,2) = 0.02$, $P = 0.89$	$r = 0.10$, $P = 0.6$	
Left entorhinal cortex	$\lambda(58,2) = 0.58$, $P = 0.45$	$r = 0.23$, $P = 0.22$	$\lambda(58,1) = 0.59$, $P = 0.44$
Right entorhinal cortex	$\lambda(58,2) = 0.74$, $P = 0.39$	$r = 0.19$, $P = 0.30$	
Left parahippocampal cortex	$\lambda(58,2) = 0.87$, $P = 0.36$	$r = 0.04$, $P = 0.85$	$\lambda(58,1) = 0.84$, $P = 0.36$
Right parahippocampal cortex	$\lambda(58,2) = 0.90$, $P = 0.35$	$r = 0.04$, $P = 0.83$	
Left amygdala	$\lambda(58,2) = 1.70$, $P = 0.20$	$r = 0.15$, $P = 0.44$	$\lambda(58,1) = 1.00$, $P = 0.32$
Right amygdala	$\lambda(58,2) = 1.43$, $P = 0.24$	$r = 0.09$, $P = 0.62$	
Left hippocampus	$\lambda(58,2) = 3.50$, $P = 0.10$	$r = 0.12$, $P = 0.58$	$\lambda(58,1) = 0.04$, $P = 0.84$
Right hippocampus	$\lambda(58,2) = 3.00$, $P = 0.10$	$r = 0.11$, $P = 0.56$	

ous studies have demonstrated decrease in temporal volumes associated with normal aging [Convit et al., 1995; Sullivan et al., 1995]. This difference can be related to methodological differences [Insausti et al., 1998] because these studies evaluated the gray matter of the temporal lobe, irrespective of the region analyzed, or a particular gyrus, including the white matter [Convit et al., 1995]. Insausti et al. [1998] observed an age-related decrease only in the temporopolar cortex. Nevertheless, according to Insausti et al. [1998] and Amaral et al. [1987], there is great interindividual variability in the pattern of sulci or gyri that are used as landmarks for the limits of the temporopolar cortex. This renders the volumetric assessment of the temporopolar cortex cumbersome and very susceptible to biological variability.

We may have not found differences on the volumes due to age or gender because of the age distribution and size of our sample or because of spatial normalization. Further studies may help to clarify this issue and determine whether there is a significant age-related decrease of temporal lobe volume in the general population.

Hemispheric Asymmetry

The volumes of the entorhinal perirhinal, temporopolar, and parahippocampal cortices, and the volumes of the hippocampi and amygdala were not affected by side. The right entorhinal cortex has been reported to be larger than the left [Insausti et al., 1998], but this has not been observed in other studies [Bernasconi et al., 1999, 2001; Juottonen et al., 1999]. Moreover, we did not find any significant asymmetry involving the amygdala or anterior temporal lobe volume (perirhinal plus temporopolar cortex). Some authors, however, have reported a larger right amygdala [Filipek et al., 1994; Watson et al., 1992], a larger left anterior temporal lobe volume [Insausti et al., 1998] or a larger right anterior temporal lobe volume [Jack et al., 1988, 1989]. To date, there is no conclusive data regarding asymmetry of temporal lobe structures in normal subjects. The inclusion of sociodemographic variables in further studies may help to clarify the degree and patterns of asymmetry that should be considered normal for certain subpopulations [Pruessner et al., 2001].

CONCLUSIONS

We have presented a tool that may be able to increase the power and reliability of volumetric studies of medial temporal lobe structures, due to the definition and confirmation of the anatomic landmarks in three different planes of MRI. High-resolution MRI in vivo studies of normal subjects and patients with different subsets of neurological diseases may help to depict the role of cortical structures in normal processes such as aging and maturation as well as in pathological conditions.

REFERENCES

Amaral DG, Insausti R, Cowan WM (1987): The entorhinal cortex of the monkey: I. Cytoarchitectonic organization. J Comp Neurol 264:326–355.

Berkovic SF, Andermann F, Olivier A, Ethier R, Melanson D, Robitaille Y, Kuzniecky R, Peters T, Feindel W (1991): Hippocampal sclerosis in temporal lobe epilepsy demonstrated by magnetic resonance imaging. Ann Neurol 29:175–182.

Bernasconi N, Bernasconi A, Andermann F, Dubeau F, Feindel W, Reutens DC (1999): Entorhinal cortex in temporal lobe epilepsy: a quantitative MRI study. Neurology 52:1870–1876.

Bernasconi N, Bernasconi A, Caramanos Z, Dubeau F, Richardson J, Andermann F, Arnold DL (2001): Entorhinal cortex atrophy in epilepsy patients exhibiting normal hippocampal volumes. Neurology 56:1335–1339.

Bland JM, Altman DG (1986): Statistical methods for assessing agreement between two methods of clinical measurement. Lancet 1:307–310.

Bronen RA, Cheung G, Charles JT, Kim JH, Spencer DD, Spencer SS, Sze G, McCarthy G (1991): Imaging findings in hippocampal sclerosis: correlation with pathology. Am J Neuroradiol 12:933–940.

Cendes F, Andermann F, Gloor P, Evans A, Jones-Gotman M, Watson G, Melanson D, Olivier A, Peters T, Lopes-Cendes I,

Leroux G (1993): MRI volumetric measurements of amygdala and hippocampus in temporal lobe epilepsy. Neurology 43:719–725.

Collins DL, Neelin P, Peters TM, Evans AC (1994): Automatic 3-D inter-subject registration of MR volumetric data in standardized Talairach space. J Comput Assist Tomogr 18:192–205.

Convit A, de Leon MJ, Hoptman MJ, Tarshish C, De Santi S, Rusinek H (1995): Age-related changes in brain: I. Magnetic resonance imaging measures of temporal lobe volumes in normal subjects. Psychiatr Q 66:343–355.

Filipek PA, Richelme C, Kennedy DN, Caviness VS Jr (1994): The young adult human brain: an MRI-based morphometric analysis. Cereb Cortex 4:344–360.

Gloor P (1997): The temporal lobe and limbic system. Oxford: Oxford University Press. p 325–527.

Insausti R, Amaral DG, Cowan WM (1987): The entorhinal cortex of the monkey: II. Cortical afferents. J Comp Neurol 264:356–395.

Insausti R, Juottonen K, Soininen H, Insausti AM, Partanen K, Vainio P, Laakso MP, Pitkanen A (1998): MR volumetric analysis of the human entorhinal, perirhinal, and temporopolar cortices. Am J Neuroradiol 19:659–671.

Jack CR Jr (1994): MRI-based hippocampal volume measurements in epilepsy. Epilepsia 35(Suppl.):21–29.

Jack CR Jr, Gehring DG, Sharbrough FW, Felmlee JP, Forbes G, Hench VS, Zinsmeister AR (1988): Temporal lobe volume measurement from MR images: accuracy and left-right asymmetry in normal persons. J Comput Assist Tomogr 12:21–29.

Jack CR Jr, Twomey CK, Zinsmeister AR, Sharbrough FW, Petersen RC, Cascino GD (1989): Anterior temporal lobes and hippocampal formations: normative volumetric measurements from MR images in young adults. Radiology 172:549–554.

Jackson GD, Berkovic SF, Tress BM, Kalnins RM, Fabinyi GC, Bladin PF (1990): Hippocampal sclerosis can be reliably detected by magnetic resonance imaging. Neurology 40:1869–1875.

Juottonen K, Laakso MP, Partanen K, Soininen H (1999): Comparative MR analysis of the entorhinal cortex and hippocampus in diagnosing Alzheimer disease. Am J Neuroradiol 20:139–144.

Lancaster JL, Glass TG, Lankipalli BR, Downs H, Mayberg H, Fox PT (1995): A modality independent approach to spatial normalization of tomographic images of the human brain. Hum Brain Mapp 3:209–223.

Margerison JH, Corsellis JA (1966): Epilepsy and the temporal lobes. A clinical, electroencephalographic and neuropathological study of the brain in epilepsy, with particular reference to the temporal lobes. Brain 89:499–530.

Milner B (1970): Memory and medial temporal regions of the brain. In: Pribram KH, Broadbent DE, editors. Biology and memory. New York: Academic Press. p 29–50.

Milner B (1972): Disorders of learning and memory after temporal lobe lesions in man. Clin Neurosurg 19:421–446.

Mishkin M (1978): Memory in monkeys severely impaired by combined but not by separate removal of amygdala and hippocampus. Nature 273:297–298.

Paus T, Otaky N, Caramanos Z, MacDonald D, Zijdenbos A, D'Avirro D, Gutmans D, Holmes C, Tomaiuolo F, Evans AC (1996): In vivo morphometry of the intrasulcal gray matter in the human cingulate, paracingulate, and superior-rostral sulci: hemispheric asymmetries, gender differences and probability maps. J Comp Neurol 376:664–673.

Penhune VB, Zatorre RJ, MacDonald JD, Evans AC (1996): Interhemispheric anatomical differences in human primary auditory cortex: probabilistic mapping and volume measurement from magnetic resonance scans. Cereb Cortex 6:661–672.

Pruessner JC, Collins DL, Pruessner M, Evans AC (2001): Age and gender predict volume decline in the anterior and posterior hippocampus in early adulthood. J Neurosci 21:194–200.

Pruessner JC, Li LM, Serles W, Pruessner M, Collins DL, Kabani N, Lupien S, Evans AC (2000): Volumetry of hippocampus and amygdala with high-resolution MRI and three-dimensional analysis software: minimizing the discrepancies between laboratories. Cereb Cortex 10:433–442.

Scoville WB, Milner B (1957): Loss of recent memory after bilateral hippocampal lesions. J Neuropsychiatry Clin Neurosci 12:103–113.

Seidman LJ, Faraone SV, Goldstein JM, Goodman JM, Kremen WS, Toomey R, Tourville J, Kennedy D, Makris N, Caviness VS, Tsuang MT (1999): Thalamic and amygdala-hippocampal volume reductions in first-degree relatives of patients with schizophrenia: an MRI-based morphometric analysis. Biol Psychiatry 46:941–954.

Sled JG, Zijdenbos AP, Evans AC (1998): A nonparametric method for automatic correction of intensity nonuniformity in MRI data. IEEE Trans Med Imaging 17:87–97.

Squire LR, Davis HP, Spanis CW (1980): Neurobiology of amnesia. Science 209:836–837.

Squire LR, Zola-Morgan S (1991): The medial temporal lobe memory system. Science 253:1380–1386.

Sullivan EV, Marsh L, Mathalon DH, Lim KO, Pfefferbaum A (1995): Age-related decline in MRI volumes of temporal lobe gray matter but not hippocampus. Neurobiol Aging 16:591–606.

Suzuki WA, Amaral DG (1994): Topographic organization of the reciprocal connections between the monkey entorhinal cortex and the perirhinal and parahippocampal cortices. J Neurosci 14:1856–1877.

Talairach J, Tornoux P (1988): Co-planar stereotactic atlas of the human brain: 3-dimensional proportional system: an approach to cerebral imaging. Stuttgart: Thieme.

Watson C, Andermann F, Gloor P, Jones-Gotman M, Peters T, Evans A, Olivier A, Melanson D, Leroux G (1992): Anatomic basis of amygdaloid and hippocampal volume measurement by magnetic resonance imaging. Neurology 42:1743–1750.

Watson C, Jack CR Jr, Cendes F (1997): Volumetric magnetic resonance imaging. Clinical applications and contributions to the understanding of temporal lobe epilepsy. Arch Neurol 54:1521–1531.

Xu Y, Jack CR Jr, O'Brien PC, Kokmen E, Smith GE, Ivnik RJ, Boeve BF, Tangalos RG, Petersen RC (2000): Usefulness of MRI measures of entorhinal cortex versus hippocampus in AD. Neurology 54:1760–1767.

Zola-Morgan S, Squire LR (1985): Medial temporal lesions in monkeys impair memory on a variety of tasks sensitive to human amnesia. Behav Neurosci 99:22–34.

Zola-Morgan S, Squire LR, Amaral DG (1986): Human amnesia and the medial temporal region: enduring memory impairment following a bilateral lesion limited to field CA1 of the hippocampus. J Neurosci 6:2950–2967.